

See discussions, stats, and author profiles for this publication at: <https://www.researchgate.net/publication/230591431>

Immobilization of Magnetic Nanoparticles onto Conductive Surfaces Modified by Diazonium Chemistry

ARTICLE *in* LANGMUIR · JULY 2012

Impact Factor: 4.46 · DOI: 10.1021/la302403z · Source: PubMed

CITATIONS

7

READS

69

6 AUTHORS, INCLUDING:



[Jonathan Quinson](#)

University of Oxford

3 PUBLICATIONS 10 CITATIONS

[SEE PROFILE](#)



[Frederic Kanoufi](#)

Paris Diderot University

119 PUBLICATIONS 1,716 CITATIONS

[SEE PROFILE](#)

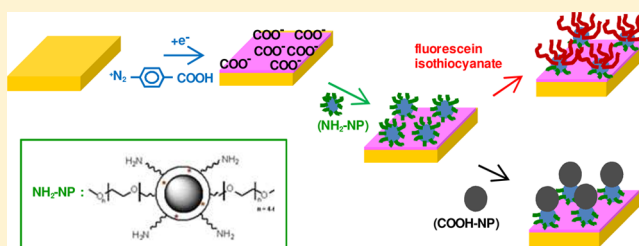
Immobilization of Magnetic Nanoparticles onto Conductive Surfaces Modified by Diazonium Chemistry

Nadia Ktari, Jonathan Quinson, Bruno Teste, Jean-Michel Siaugue, Frédéric Kanoufi, and Catherine Combellas*

Physicochimie des Electrolytes, Colloïdes et Sciences Analytiques, ESPCI ParisTech, CNRS UMR 7195, 10 rue Vauquelin, Paris, F-75231, France

Supporting Information

ABSTRACT: Core-shell $\gamma\text{-Fe}_2\text{O}_3\text{@SiO}_2$ nanoparticles (NPs) substituted by PEG and NH_2 groups may be immobilized on metal surfaces (glassy carbon or gold) substituted by 4-carboxyphenyl groups through electrostatic interactions. Such immobilization is evidenced by (i) IRRAS owing to the Si-O band, (ii) SEM images, which show that the surface coverage by the NPs is nearly 100%, and (iii) the NPs film thickness measured by ellipsometry or AFM, which corresponds to about one NPs monolayer. Such NPs film is permeable to redox probes, which allows us to propose electrochemical methods based on direct or local measurements as a way to inspect the NPs assembly steps through their ability to alter mass and charge transfer. This process also applies to patterned polystyrene surfaces, and selective immobilization of NPs substituted by amino groups was carried out onto submillimeter patterns obtained by local oxidation. Biological applications are then expected for hyperthermia activation of the NPs to trigger cellular death. Finally, some tests were performed to further derivatize the immobilized NPs onto surfaces through either a covalent bond or electrostatic interactions. Future work will be dedicated to the recovery of such Janus NPs from the substrate surface.



INTRODUCTION

Over the past few years, the field of nanomaterials has largely expanded, due to the special physical and chemical properties of nanostructures that strongly contrast with those of bulky materials.¹ The immobilization of nanoparticles (NPs) assemblies onto material surfaces along one, two, or three dimensions has drawn special interest, due to various applications in catalysis, optics, electronics, biochemistry, detection, and so forth.^{2–10}

Different strategies are reported to immobilize a nanostructure onto a surface, depending on whether the surface or the NP is functionalized. Regarding surface modification, thiols, pyridines, amines, or carboxylic functions that are prone to interact with NPs have been used. For example, the modification of glass surfaces by silanes substituted by a thiol function allowed improvement of the adhesion of a gold film deposited under vacuum.¹¹ Such a strategy was extended to immobilize silver or gold or other metal NPs onto glass, silicon, and ITO surfaces.^{12–15}

In the same way, the functionalization of NPs may be directed so that the new function is prone to interact with original surface functions.^{16–19} For example, ω -alkene-1-thiol modified gold NPs were immobilized onto a (111) silicon surface owing to Si-C covalent bonding.¹⁹ Electrostatic interactions between the NPs and the surface may also be used, for example, via the layer by layer adsorption of polycationic/polyanionic systems.^{20–24} Let us mention the layer by layer assembly of silica NPs and polydimethyl diallyl

ammonium, under pH control to optimize the charge density of both the polyelectrolyte and the NPs surface.^{22,23}

In this context, we report the immobilization of magnetic NPs onto metal surfaces modified by diazonium chemistry. On one hand, magnetic nanoparticles are promising vectors used in clinical treatments, bioassays, or for the design of surfaces or materials presenting magnetic or catalytic properties. In this respect, the controlled immobilization of such NPs on surfaces and their possible functionalization is an important aspect. On the other hand, electrografting by cathodic reduction of diazonium salts allows one to obtain compact functional grafted aryl layers with tunable charge transfer properties onto various surfaces such as glassy carbon,²⁵ metals,²⁶ semiconductors,²⁷ metal oxides, and carbon nanotubes,²⁸ as well as diamond²⁹ and carbonized Teflon.³⁰ To the best of our knowledge, such a process has rarely been used to immobilize NPs.^{31–34} It could be highly beneficial due to its simplicity and the versatility of the functional groups, which can be introduced with the help of diazonium chemistry. First, core-shell $\text{Fe}_2\text{O}_3\text{@SiO}_2$ NPs functionalized by amino functions and poly(ethylene glycol) (PEG) chains will be immobilized onto model surfaces (carbon, gold). The process will be extended to polymeric surfaces such as patterned surfaces of polystyrene that were previously shown to allow discrimination between different

Received: June 13, 2012

Revised: July 23, 2012

Published: July 31, 2012

types of biological cells.³⁵ We have focused on magnetic NPs, as their deposition onto a surface is a key step in the design of thermosensitive surfaces useful for hyperthermal biological cell actuation.³⁶ Finally, attempts will be made to functionalize the immobilized NPs to get Janus NPs; such NPs present exceptional properties regarding the control of the assembly and the ability to tune their surface chemistry and also their optic and electronic properties.³⁷ The different surface assembling steps will be followed by the confrontation of different surface analytic methods with indirect inspection of electrochemical charge transfer processes.

■ EXPERIMENTAL SECTION

Chemicals. *N*-(3-Dimethylaminopropyl)-*N*-ethylcarbodiimide hydrochloride (EDC), *N*-hydroxysulfosuccinimide sodium salt (NHS), 3-(*N*-morpholino)propanesulfonic acid sodium salt (MOPS), Tween 20 (polyoxyethylene (20) sorbitan monolaurate), phosphate buffered saline, pH 7.4 (PBS), fluorescein, fluorescein isothiocyanate (FITC), and 4-carboxyphenyl diazonium tetrafluoroborate were purchased from Sigma–Aldrich; potassium ferrocyanide trihydrate (97%) was from Janssen Chimica; and potassium chloride (99.5%) was from Prolabo. Aqueous solutions were made up in high-purity Millipore water of resistivity >18 MΩ cm.

Functionalized Core–Shell $\gamma\text{Fe}_2\text{O}_3/\text{SiO}_2$ Nanoparticles Synthesis. Magnetic core–shell NPs ($\gamma\text{Fe}_2\text{O}_3/\text{SiO}_2$) functionalized with poly(ethylene glycol) chains and amino or carboxylic acid groups (respectively, NH_2 -NPs or COOH -NPs) were synthesized using a previously described procedure.³⁸ Briefly, Fe^{2+} and Fe^{3+} ions were coprecipitated under alkaline conditions to give maghemite NPs ($\gamma\text{Fe}_2\text{O}_3$, 7 nm diameter).³⁹ The obtained NPs were coated by citrate anions, then dispersed and stabilized in a pH 7 aqueous solution. Then, they underwent a first step of encapsulation in silica shells by the sol–gel process. During this step, it is possible to incorporate a fluorophore such as fluorescein within the silica layers (NH_2 -FNPs). In a second step, the silica shell was functionalized by simultaneous condensation of a silica amino-derived compound and a silica PEG-derived compound (molar ratio 1/3). The amine-modified particles NH_2 -NPs were converted to carboxylic acid-modified NPs, COOH -NPs, via an overnight reaction with 700 equiv of succinic anhydride (relative to the amine function quantity). One can consider that all amino groups are converted into carboxylic acid groups by reaction with a large excess of succinic anhydride.⁴⁰ PEG moieties (4–6 ethylene glycol) provide steric stabilization to the system, while amino or carboxylic acid functions ensure the electrostatic stability and are appropriate sites for grafting.

Such particles are named NH_2 -NPs (NH_2 -FNPs when a fluorophore has been incorporated during the synthesis of NH_2 -NPs) and COOH -NPs (idem for COOH -FNPs). Their physical size is 35 ± 6 nm. The relative amine coverage (0.3 amine functions per nm^2 , i.e., $\sim 10^3$ NH_2 functions per NH_2 -NP) was estimated with the ninhydrin colorimetric assay, as previously described.⁴¹ The NPs solutions (approximately 3×10^{14} NPs mL^{-1}) are stable for months. At pH = 7.4, NH_2 -NPs and COOH -NPs are, respectively, positively and negatively charged, due to amino and carboxylic functions.

Electrodes and Gold Plates. For cyclic voltammetry measurements, 1 mm disk gold and glassy carbon electrodes were used. They were polished with a 0.04 μm alumina slurry on a polishing cloth, using a Presi Mecatech 234 polishing machine, and rinsed in Milli-Q water.

1 \times 1 cm^2 gold-coated wafers (Aldrich, 1000 Å coating) were cleaned with a “piranha” solution (1:3 v/v $\text{H}_2\text{O}_2/\text{H}_2\text{SO}_4$) for 10 min at 80 °C, and rinsed under sonication for 10 min in Milli-Q water. Before modification, the plates were dried under a stream of nitrogen. *Caution: piranha solutions are highly aggressive and should be handled with full protection, gloves, mask, and so forth.*

Preparation of 4-Carboxyphenyl Grafted Gold Wafers. The electrochemical grafting of 4-carboxyphenyl diazonium was performed in acetonitrile containing 2 mM 4-carboxyphenyl diazonium

tetrafluoroborate and 0.1 M $\text{NBu}_4^+\text{BF}_4^-$ as supporting electrolyte. The grafting procedure was performed by chronoamperometry.

Preparation of Polystyrene Grafted Gold Wafers. They were obtained as previously described⁴² by a two-step procedure: (i) electrografting of a bromobenzyl moiety onto the gold wafer and (ii) ATRP polymerization of styrene from the surface.

The electrochemical grafting of $^+\text{N}_2\text{--C}_6\text{H}_4\text{--CH}(\text{CH}_3)\text{--Br}^{43}$ onto the gold wafer was achieved by chronoamperometry for 300 s, at a potential 300 mV more negative than the diazonium salt peak potential. The gold wafer was then thoroughly rinsed under sonication in deaerated acetone.

CuBr (390 mg, 2.7 mmol) and a piece of the initiator grafted gold or silicon wafer were placed into a 100 mL Schlenk flask equipped with a magnetic stirring bar and sealed with a rubber septum and deoxygenated by a nitrogen flow. 2,2′-Dipyridyl (1.17 g, 7.5 mmol) was placed into a two-neck round-bottom flask, and the flask was evacuated and backfilled with nitrogen. To this flask, 10 mL of toluene was added and this solution was stirred for 20 min under nitrogen. The resulting solution was transferred through a cannula to the Schlenk flask. In a second two-neck round-bottom flask, styrene (24 mL, 210 mmol) was deoxygenated by a nitrogen flow. The monomer solution was transferred through a cannula, and the flask was held at 110 °C. After several hours, the substrate was removed from the flask, washed with dichloromethane, and sonicated in toluene and dichloromethane.

Nanoparticle Immobilization. All delivered stock solutions of NPs were diluted three times in a PBS solution containing 1% Tween 20. The grafted carboxylic functions were deprotonated using a pH 9 buffer solution (100 mL of 0.025 M $\text{Na}_2\text{B}_4\text{O}_7 + 9.2$ mL of 0.1 M HCl) for 5 min. Then, 30 μL of the NP diluted solution was deposited onto the substrate surface for ~ 1 min, and finally, the surface was rinsed with water and dried under a stream of N_2 . The grafted gold surface is designated by $\text{Au-NH}_2\text{-NP}$.

Immobilized Nanoparticle Functionalization. The $\text{Au-NH}_2\text{-NP}$ surface was functionalized either by molecules (fluorescein or fluorescein isothiocyanate) or by fluorescent COOH -FNPs.

Nanoparticle Interaction with Fluorescein. Fluorescein was dissolved into a few drops of acetone, then in phosphate buffer (1 g/L PBS, pH 7.4). This solution was reacted with the $\text{Au-NH}_2\text{-NP}$ surface for 10, 20, or 40 min or 24 h, and then the substrate was rinsed in water.

Nanoparticle Functionalization by Fluorescein Isothiocyanate (FITC). The same dilution procedure as for fluorescein was used, with pH = 7.4, even if the dissolution is known to be favored at pH 9. Indeed, the silica shell of the NP is attacked at a basic pH. The $\text{Au-NH}_2\text{-NP}$ surface was reacted with the FITC solution overnight and then washed with water.

Nanoparticle Functionalization by COOH -FNPs. The COOH -FNPs were diluted 3 times in PBS + 1% Tween. The $\text{Au-NH}_2\text{-NP}$ surface was reacted with the COOH -FNPs for 10 min in a neutral PBS solution. This favored electrostatic interactions between the two types of NPs. To favor a covalent bond, the $\text{Au-NH}_2\text{-NP}$ surface was reacted overnight in MOPS (neutral buffered solution) with 20 μL of the stock solution of COOH -FNP, 20 μL of 5 mg/mL EDC, and 20 μL of 5 mg/mL NHS and then washed with water.

Electrochemical Procedures. Cyclic voltammetric experiments were performed with a classical three-electrode setup with a bare Pt wire counter-electrode and a saturated calomel electrode (SCE) reference.

SECM experiments were performed with a homemade SECM described previously.⁴⁴ Approach curves were obtained with a microelectrode tip made of a 25- μm -diameter Pt wire insulated in glass (RG = 5) assembled with a 250- μm -diameter Pt counter electrode and a 250 μm Ag/AgCl reference electrode along an already described procedure.⁴⁵ This three-electrode assembly was positioned in a 10–20 μL droplet of electrolytic solution. The measurement then consisted of characterizing a few mm^2 of the substrate. The parallel positioning and approach curves were obtained using a 5 mM solution of a redox mediator ($\text{Fe}(\text{CN})_6^{4-}$, 4K^+) with 0.1 M KCl in water, as reported elsewhere.⁴⁶ The determination of the apparent heterogeneous electron transfer rate constants to a redox probe through the

modified electrode surfaces was obtained from kinetics measurements by cyclic voltammetry or SECM. By SECM, it consists of fitting the experimental approach curves at the unbiased substrate (tip current variations with the tip–substrate separation distance) with available analytical expressions.⁴⁷ By cyclic voltammetry, it consists of estimating the difference between the anodic and cathodic peak potentials and comparing this value to simulated values according to a slow electron transfer process obtained through Digisim.

SECM lithography on polystyrene was performed on a Petri dish surface with a 250 μm Pt tip. The patterns were obtained by local oxidation of the polystyrene surface by Ag(II) electrogenerated at the SECM electrode using a previously described procedure.⁴⁸ A two-electrode configuration was used (with a 250- μm -diameter Pt wire counter electrode). The tip was biased at 2.09 V vs Pt and moved at 5 $\mu\text{m/s}$ above the polystyrene surface (tip–surface distance: 10 μm).

Potentials and currents were controlled by a CH660 potentiostat (CH Instruments, Austin, TX, USA).

FT-IRRAS. FT-IRRAS spectra were recorded with a JASCO FT/IR-6100 type A spectrometer equipped with a liquid-nitrogen-cooled MCT detector and with a grazing angle reflectance accessory (RAS-PRO410-H), which allows FT-IRRAS measurements with a grazing angle of 85°. Each spectrum results from the accumulation of 500 interferograms with a 4 cm^{-1} resolution. The spectrometer is purged with dry and carbon dioxide free air for at least 10 min before recording the spectrum. Residual CO_2 and H_2O signals were automatically suppressed from the spectra. The profiles were recorded with an IRRAS Jasco IRT 700S microscope, using a 40 \times 40 μm^2 beam size and 800 accumulations with a spectral resolution of 4 cm^{-1} .

Thicknesses. Thicknesses of the films deposited onto gold surfaces were measured with a mono wavelength ellipsometer Sentech SE400. The following values were taken for gold: $n_{\text{sub}} = 0.153$, $k_{\text{sub}} = 3.567$. These values were measured on clean surfaces before grafting, and the film thicknesses were determined from the same plates after modification, taking $n_i = 1.46$ and $k_i = 0$ for the layer.

AFM Images. AFM measurements were performed using a 5100 atomic force microscope (Agilent technologies - Molecular Imaging) operated in dynamic tip deflection mode (acoustic alternating current mode, AAC). All AFM experiments were carried out using silicon probes (Applied NanoStructures-FORT) in the tapping mode with 3 N m^{-1} spring constant at 69 kHz. The images were scanned in topography, amplitude, and phase mode with a resolution of 512 \times 512 pixels and are representative of 1 \times 1 μm^2 regions over different locations on the studied surfaces.

RESULTS AND DISCUSSION

NH₂–NPs Immobilization onto a Glassy Carbon Electrode. The electrode surface was grafted by cathodic reduction of 4-carboxyphenyl diazonium in acetonitrile. Such reduction leads to a grafted organic film that presents pinholes. We have previously shown⁴⁹ that, because of the thickness of this organic layer, outer sphere electron transfers between a redox probe and the electrode were limited to the probe direct diffusion transfer through the pinholes whose sizes are larger than that of the probe. Other electron transfer modes such as tunneling are negligible.

Different theoretical approaches are reported in the literature to model the electron transfer to a redox probe through pinholes,^{50–52} which are assumed as simple disks that are uniformly distributed at the electrode surface or through electrodes with randomly distributed patches of defects.^{53,54} Briefly, the electrochemical response of partially covered electrodes depends mainly on the size of the defects and the distance separating two defects (the defects density); both dimensions are compared to the size of the diffusion zone inspected by the electrochemical technique in order to make the defects behave as individual or overlapping sources. Typically, an electrode covered with an insulating film

presenting large (micrometric) defects shows a cyclic voltammetric response with linear diffusion characteristics (peak-shaped) similar to the bare uncovered electrode, but with a lower current peak height as a result of the lower available surface area of the defect sites.⁵⁰ When decreasing the defect dimension, the shape of the electrochemical response may change. When the defects can be considered as small independent hemispherical sources, the CV response becomes steady-state (sigmoidal instead of peak-shaped). While decreasing the interdefect distance, the response becomes peak-shaped; it is the same as for the uncovered electrode, but with an apparently lower electron transfer rate: the electrochemical system becomes less reversible as a higher separation potential is observed between the anodic and cathodic peaks for the redox probe. In this latter case, the surface coverage, θ , of the covering layer can be obtained from the apparent electron transfer rate at the electrode. Amatore showed that it is given by⁵¹

$$k_{\text{app}} = k^\circ(1 - \theta) \quad (1)$$

where k° and k_{app} represent the apparent electron transfer rates, respectively, at the bare and grafted surfaces. Then, for a quasi-reversible system, the determination of the apparent electron transfer rate constant is obtained using cyclic voltammetry, as depicted by Nicholson, from the variation of the anodic and cathodic peak potential differences, ΔE_p , with the CV potential scan rate, v .⁵⁵

This strategy is used here to follow the electrode surface coverage during the successive steps of the assembly at the surface. The apparent electron transfer rate of the electrode before (k° in eq 1) and after a functionalization step (k_{app} in eq 1) are measured and compared in light of eq 1, as partial coverage of the surface ($\theta_{\text{after/before}}$ in eq 1) due to the functionalization step.

First, the grafting of a bare electrode is addressed with a –COOH layer. After rinsing in acetone and water, the grafted electrode was transferred into an aqueous solution containing the redox probe (ferrocene methanol or potassium ferrocyanide). With ferrocene methanol, the cyclic voltammogram for the grafted electrode is identical to that obtained for bare carbon. This results from the pK_a of the grafted aryl-COOH/COO[–] acid/base couple that was estimated as 2.8 with a grafted gold electrode.⁵⁶ Due to the carboxylic functions, the organic film is negatively charged and hydrophilic, which makes it permeable to ferrocene methanol. Therefore, such a probe cannot be used to evidence surface modifications of the electrode.

Because of electrostatic repulsion, ferrocyanide, that is negatively charged, should be less prone to permeation inside the organic film than ferrocene methanol. Indeed, when the carbon electrode had been grafted by –COOH during the reduction of the diazonium salt at –0.300 V for 600 s, the current gets negligible (compare curves a and e in Figure 1A for, respectively, bare and grafted glassy carbon), which proves that the electrode has nearly been totally passivated. In order to propose an indirect electrochemical method based on electron transfer kinetics attenuation to inspect the electrode surface coverage during the layer-by-layer surface assembly, the electrode must not be completely blocked in the first grafting step. Therefore, a thinner anchoring –COOH layer was grafted onto the electrode from its polarization at a more positive potential and for a shorter time. Suitable results were obtained with a –0.050 V potential for a 0.25 s treatment. Then, the

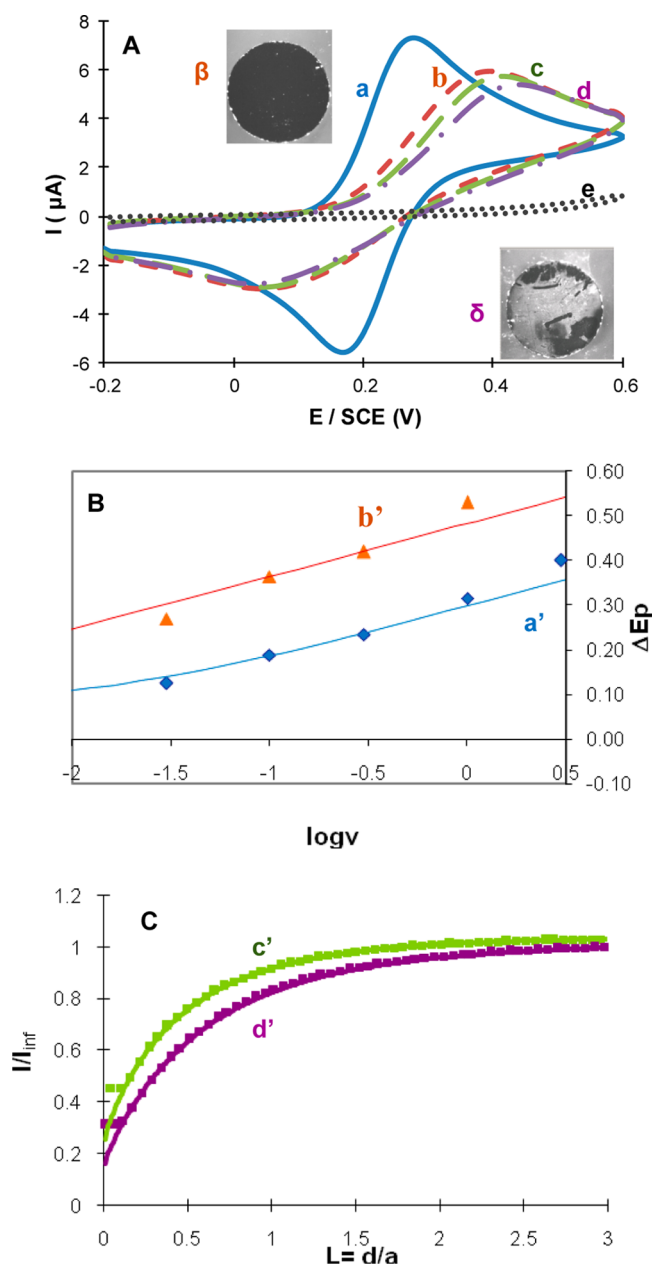


Figure 1. Electrochemical evidence of successive surface modifications. (A,B) Cyclic voltammetry of a glassy carbon electrode (diameter = 1 mm) in 5 mM $\text{Fe}(\text{CN})_6\text{K}_4$ + 0.1 M KCl. (C) SECM. (a,a') bare. (b,b') Functionalized by 4-carboxyphenyl diazonium at $E = -0.050$ V for 0.25 s, then immersed into either (c) a reference solution (Tween + PBS + MOPS) or (d) a NH_2 -FNPs solution. (e) Functionalized by 4-carboxyphenyl diazonium at $E = -0.300$ V for 600 s. β and δ are the fluorescence images corresponding, respectively, to (b) and (d). (a',b'): \blacklozenge , \blacktriangle experimental points; the curves are simulated by $k^0 = 2 \times 10^{-4}$ cm/s (blue line) and $k_s = 1.2 \times 10^{-3}$ cm/s (orange line). (C) SECM approach curves in 2 mM solution of $\text{Fe}(\text{CN})_6^{4-}$ toward a carboxyphenyl modified gold surface immersed into (c') a PBS + Tween + MOPS solution (d') containing $\gamma\text{-Fe}_2\text{O}_3@/\text{SiO}_2\text{NH}_2$ -FNPs. Experimental points (green \blacksquare , purple \blacksquare), and theoretical lines with $k_s = 0.0031$ (c') and 0.00177 (d').

electrode gets partially blocked upon grafting, as evidenced by the higher ΔE_p compared to the bare electrode (curves a and b in Figure 1A). The current intensity is also decreased by 20% upon this grafting; however, it corresponds to the predicted variation (21.4%)⁵⁷ for the transition from a reversible (curve

a) to an irreversible (curve b) electron transfer process. These observations then indicate that the grafting yields the formation of a layer with nanostructured-size defects.

The variation of ΔE_p with the scan rate, v , is represented in Figure 1B (curves a' and b' for, respectively, bare, GC, and $-\text{COOH}$ grafted, $\text{GC}-\text{COOH}$, carbon). Using the electron transfer rates deduced from the fitting of the curves ($k_{\text{GC}}^0 = 1.2 \times 10^{-3}$ and $k_{\text{app,GC}-\text{COOH}} = 2.0 \times 10^{-4}$ cm/s for, respectively, GC and $\text{GC}-\text{COOH}$ surfaces) and eq 1 gives $\theta_{\text{GC}-\text{COOH/GC}} = 85 \pm 5\%$ for the electrode surface coverage by the seeding $-\text{COOH}$ layer. The electron transfer attenuation introduced by the COOH layer corresponds to altered mass transfer through nanometer size defect sites.

Following the modification step, the grafted electrode, $\text{GC}-\text{COOH}$, was deprotonated in a buffered solution of sodium tetraborate ($\text{Na}_2\text{B}_4\text{O}_7$, pH 9) and then immersed for a short time (~ 1 min) into a solution containing the fluorescent NH_2 -nanoparticles (NH_2 -FNPs). That solution is made of MOPS buffer at pH 7.4 and also contains a surfactant (Tween) to avoid NPs aggregation. Such solution without the NPs has a slight blocking effect on the electrode. The $\text{GC}-\text{COOH}$ electrode, after deprotonation and further immersion into such solution, is denoted GC and presents a lower electron transfer rate than $\text{GC}-\text{COOH}$, as observed in Figure 1 (curve c, $k_{\text{app,GC}} = 1.7 \times 10^{-4}$ cm/s compared to $k_{\text{app,GC}-\text{COOH}} = 2.0 \times 10^{-4}$ cm/s) with $<4\%$ current intensity change. Even though the surfactant and MOPS may adsorb on any part of the electrode surface (the part covered with the organic seeding layer and the defects), the measurement of k_{app} only interrogates the defect population where the electron transfer is supposed to occur. For such layer by layer assembly of small molecules, Amatore's model for partially blocked electrode surfaces applies and allows characterization, through the decrease in k_{app} , of a statistical filling of the defect sites. Based on eq 1, the immersion in the surfactant solution yields a $\theta_{\text{GC/GC}-\text{COOH}} = 15\%$ coverage of the pores.

Then, NH_2 -FNPs are immobilized on the GC surface, yielding the $\text{GC}-\text{NH}_2$ -FNP surface whose electrochemical response is also inspected by CV (Figure 1A, curve d). The immobilization of the NH_2 -FNPs also results in (i) the blocking of the electron transfer rate (curve d, $k_{\text{app,GC}-\text{NH}_2\text{-FNP}} = 1.2 \times 10^{-4}$ cm/s), but also (ii) in a 11% decrease of the current intensity. The experiment was repeated 5 times and the results were reproducible. The presence of the NH_2 -FNPs is attested by fluorescence images of the grafted electrode surface before and after immersion into the NPs solution (Figure 1A, compare images β and δ , respectively).

Unlike molecular adsorption, which typically alters the electron transfer properties at an electrode, the assembly of bigger insulating spherical objects on an electrode surface is expected to mainly affect the mass transfer of a redox probe to the electrode surface.^{53,58} The mass transport then occurs within the tortuous void space of the NPs layer. The diffusivity of the redox probe within the assembly of NPs, D_{NP} , is expected to be lower than its diffusivity in solution, D_{sol} , and both quantities are related by

$$D_{\text{NP}} = (\varepsilon/\tau)D_{\text{sol}} \quad (2)$$

where ε is the void volume fraction available for diffusion and τ is the so-called tortuosity. The observed decrease in peak current is indicative of a hindering of the mass transport to the electrode by the NPs assembly. The peak current, i_p , for a

diffusion-controlled electrochemical reaction gives access to the diffusivity, as i_p is predicted to be proportional to the square root of v and of the apparent diffusion coefficient, D .⁵⁷ The processes under scrutiny here are indeed diffusion controlled, as their i_p values are proportional to the square root of v at the different assembled electrodes. The decrease in i_p detected when going from GC to GC-NH₂-FNPs due to the NPs immobilization is likely related to a decrease in the redox probe diffusivity within the NP layer, D_{NP} . The 11% current decrease implies that $(D_{NP}/D_{sol})^{1/2} = 0.89$ and then that D_{NP} is 78% lower than the diffusivity in solution, D_{sol} . It was demonstrated in layered assemblies of spheres that the variation of the diffusivity can be predicted from the geometrical consideration of the void volume accessible for diffusion and of the tortuosity of the assembly. 3D modeling also showed that tortuosity in a monolayer of spheres is close to 1.⁵⁸ According to eq 2, $D_{NP} \approx \epsilon D_{sol}$ and the void volume unoccupied by the NPs is $\epsilon = 78\%$, or equivalently, the volume occupied by the NPs is 22%.

Associated with the predicted change in mass transfer, the NPs assembly is also associated with a 30% decrease in the charge transfer rate for the GC-NH₂-FNP electrode compared to GC. Based on eq 1, this means that the NPs assembly also yields a relative filling of $\theta_{GC-NH_2-FNP/GC} = 30 \pm 5\%$ of the defects present on GC or a relative filling of $\theta_{GC-NH_2-FNP/GC-COOH} = 60\%$ of the defects of GC-COOH. This alteration of k_{app} is not predicted for solid spheres immobilized on an electrode surface. It could result from the interaction of the pendant molecular chains grafted on the NPs within the pores of the COOH-terminated nanometer-thin layer electrografted on the electrode.

Similar experiments for the electrografting of a gold electrode instead of glassy carbon were unsuccessful, since the electrochemical response turned to that of bare gold as the number of voltammetric scans increased. Such behavior has already been reported and is attributed to the restructuring of the layer and the loss of aryl groups upon scanning or sonication.⁵⁹

NH₂-FNPs Immobilized onto a Gold Wafer. The immobilization of the NH₂-FNPs onto gold wafers (Au-NH₂-FNP) was evidenced by SECM, SEM, and IRRAS.

Details for the procedure and data analysis obtained from indirect (SECM) electrochemical characterizations are provided in the Experimental Section.

Figure 1C presents the SECM approach curves for Fe(CN)₆⁴⁻ above the grafted electrode that has been previously immersed into a PBS + Tween + MOPS solution in the absence or presence (Figure 1C, respectively, curves c' and d') of the NH₂-FNPs. The blocking effect is characterized by the ET kinetic rate constant estimated by fitting the experimental approach curves with available analytical solutions for irreversible finite kinetics at the substrate.⁴⁷ Both approach curves are close to the negative feedback curve characteristic of an insulating surface. They are fitted by $k_{app,Au} = 3.1 \times 10^{-3}$ (c') and $k_{app,Au-NH_2-FNP} = 1.8 \times 10^{-3} \text{ cm s}^{-1}$ (d'), respectively. These SECM measurements describe the change in mass-transfer rate at the electrode. They account for both the transport within the porous electrografted layer structure (mainly provided by $k_{app,Au}$) and through the layer of assembled NPs. Considering that the NPs only hinder the electrode surface and allow mass transfer within the void volume, the observed change in k_{app} indicates a change in diffusivities. Since for mass-transfer controlled processes, k_{app} is proportional to D ,^{42,60,61} eq 2 suggests that the void volume $\epsilon > k_{app,Au-NH_2-FNP}/k_{app,Au} = 0.58$

± 0.05 or equivalently that the volume occupied by the NPs on the electrode is $<42 \pm 5\%$, which is comparable to that obtained by cyclic voltammetry on a glassy carbon electrode.

The NH₂-FNPs immobilization was also evidenced by SEM on bare and modified surfaces. Despite the well-known affinity between amines and gold, the analysis of a gold surface put in contact with the NH₂-FNPs shows a very low amount of immobilized NPs (Figure 2A). Conversely, a compact monolayer of particles is present on a grafted gold electrode

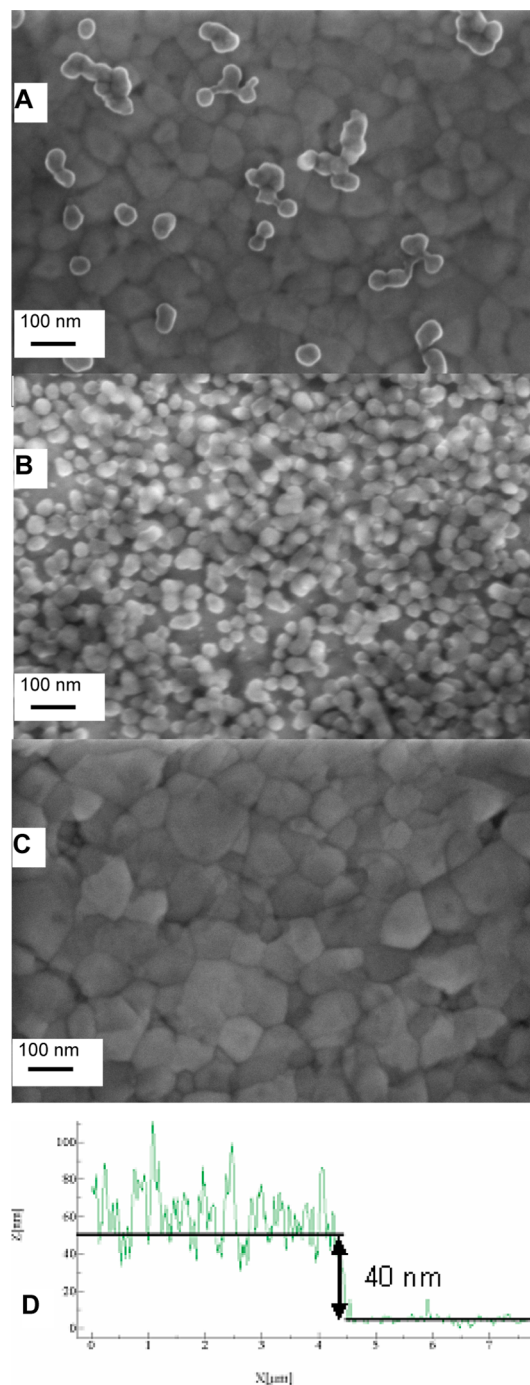


Figure 2. (A,B) SEM images for $\gamma\text{-Fe}_2\text{O}_3@SiO_2$ NPs immobilized onto either a bare gold wafer (A) or a carboxyphenyl modified gold wafer (B). (C) Reference image for a bare gold wafer. (D) AFM profile at the interface between bare gold (right) and NPs immobilized onto gold modified by carboxyphenyl (left).

surface (Figure 2B), with a $\text{NH}_2\text{-FNPs}$ surface coverage, $\theta_{\text{S,Au-NH}_2\text{-FNP}} = 90 \pm 5\%$. Their diameter is ~ 40 nm, which agrees well with the 35 ± 6 nm expected diameter for such $\text{NH}_2\text{-FNPs}$. In some places, a less homogeneous layer can be observed on top of the monolayer. The immobilization of the NPs was confirmed by AFM images, which show a dense NPs film (see Figure SI-1, Supporting Information), characterized by a ~ 40 nm step present on the AFM profile (see Figure 2D).

This demonstrates the important role of the organic film and carboxyl groups in the $\text{NH}_2\text{-FNPs}$ adhesion process on a surface. It should be noted that the surface of a gold wafer observed by SEM (Figure 2C) shows terraces. The step heights of these terraces are sometimes close to the size of the $\text{NH}_2\text{-FNPs}$, making it difficult in some cases (of high density) to estimate the NPs surface coverage. With a grafted glassy carbon electrode, similar features are observed by SEM (see Figure SI-2, Supporting Information).

Onto glassy carbon, SEM allowed estimate $\theta_{\text{S,GC-NH}_2\text{-FNP}} = 60 \pm 5\%$.

The values obtained for the electron transfer rates and the surface coverages or void volumes estimated by the different methods are reported in Table 1 for both glassy carbon and gold.

Table 1. Mass and Charge Transfer Blocking Properties of the Assembled Substrates

substrate	electrochemical characteristics ^a	surface coverage (θ) or void volume (ϵ)	
		from electrochemistry	from SEM
GC	$k_{\text{GC}}^{\circ} = 1.2 \times 10^{-3b}$; $i_p = 7 \mu\text{A}$		
GC-COOH	$k_{\text{app,GC-COOH}} = 2.0 \times 10^{-4b}$; $i_p = 5.6 \mu\text{A}$	$\theta_{\text{GC-COOH/GC}} = 85 \pm 5\%^d$	
GC-COOH-Tween = GC	$k_{\text{app,GC}} = 1.7 \times 10^{-4b}$; $i_p = 5.5 \mu\text{A}$	$\theta_{\text{GC/GC-COOH}} = 15 \pm 5\%^d$	
GC-NH ₂ -FNP	$k_{\text{app,GC-NH}_2\text{-FNP}} = 1.2 \times 10^{-4b}$; $i_p = 4.9 \mu\text{A}$	$\theta_{\text{GC-NH}_2\text{-FNP/GC}} = 30 \pm 5\%^d$; $\epsilon = 78\%^e$	$\epsilon = 60\%^f$
Au-COOH-Tween = Au	$k_{\text{app,Au}} = 3.1 \times 10^{-3c}$		
Au-NH ₂ -FNP	$k_{\text{app,Au-NH}_2\text{-FNP}} = 1.8 \times 10^{-3c}$	$\epsilon = 58\%^e$	$\epsilon = 40\%^f$

^aPeak current and k_{app} , apparent charge transfer rate constant, in cm s^{-1} . ^bFrom peak potential separation in CV. ^cFrom SECM approach curves. ^dFrom eq 1, $k_{\text{app,new}}/k_{\text{app,0}} = (1 - \theta_{\text{new/0}})$, and (b). ^eFrom (2) using $\tau = 1$, D are obtained from ratio of CV peak current and of SECM k_{app} values before and after NPs assembly. ^fFrom geometrical consideration and from the SEM estimation of the NPs surface coverage.

The surface coverages estimated by SEM can be converted into a void volume from geometrical considerations. It is assumed that the NPs, of radius r_s as estimated by SEM, are arranged in an incomplete monolayer array of n particles per electrode surface unit. The surface (2D) fractional occupancy estimated by SEM is $\theta_s = \pi r_s^2 n$. For a monolayer of NPs, one can estimate the volume capacity of the layer, as a cylinder of unit electrode surface and $2r_s$ height $V_t = 2r_s$ in which the NPs assembly occupies a volume $V_{\text{NP}} = 4\pi r_s^3 n/3$. The fractional volume occupied by the NPs is then $V_{\text{NP}}/V_t = 2\pi r_s^2 n/3 = 2\theta_s/3$ or the void volume $\epsilon = 1 - 2\theta_s/3$ yielding $\epsilon = 0.6$ and 0.4 , respectively, for GC and Au substrates. One can then compare

the void volume as obtained from both electrochemical (cyclic voltammetry or SECM) and SEM measurements (respectively, 78% and 60% for glassy carbon, and 58% and 40% for gold). It suggests that electrochemistry underestimates the volume occupied by the NPs, which could be due to a lower apparent value of the NPs radius. This can be attributed to possible transport of the redox probe within the NP polyelectrolyte shell facilitated by the positive charges of the $\text{NH}_2\text{-FNPs}$ at neutral pH. Such permeation and transport of redox probes in nanometer thin polyelectrolyte or polymer brush coatings have already been observed and quantified.^{42,49}

This indirect mass transfer characterization by local (SECM) or global (cyclic voltammetry) electrochemical characterization provides a fast and efficient way to estimate the coverage of conducting surfaces with insulating magnetic NPs. Similarly, combined optical characterization of the surfaces by IRRAS and ellipsometry also provides a systematic and reliable means to depict NPs assemblies on surfaces.

The IRRAS spectrum of a gold wafer modified by chronoamperometry for 300 s at -0.6 V by 4-carboxyphenyl diazonium indicates the presence of carboxyl groups on the surface (not shown). Ellipsometry of the same sample shows a uniform $\sim 20\text{--}30$ Å organic film thickness, that corresponds to ~ 5 layers of diazonium (phenyl ring). After immobilization of the $\text{NH}_2\text{-FNPs}$, the average layer thickness increases to $\sim 20\text{--}40$ nm (taking $n = 1.46$ for the NPs layer refractive index), in good agreement with the NPs size, and also with SEM and AFM results.

The efficiency of the electrode modification to immobilize the $\text{NH}_2\text{-FNPs}$ was evidenced by IRRAS. Figure 3 represents

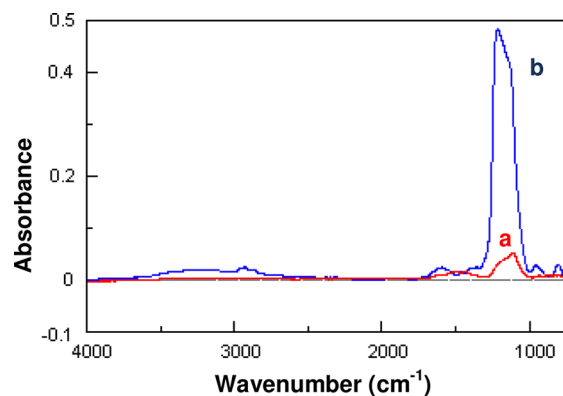


Figure 3. IRRAS spectra of $\gamma\text{-Fe}_2\text{O}_3\text{@SiO}_2$ NPs immobilized onto a carboxyphenyl modified gold wafer (a) or a bare gold wafer (b).

the IRRAS spectra for a bare (a) and a grafted (b) gold wafer that were immersed into a $\text{NH}_2\text{-FNPs}$ solution. Both spectra present a large band between 1000 and 1200 cm^{-1} that is characteristic of the Si-O stretching⁶² and corresponds to the silica NPs shell. Such band is ~ 10 times more intense for the grafted wafer (b). As expected, the $\text{NH}_2\text{-FNPs}$ are largely more efficiently immobilized onto the grafted electrode.

$\text{NH}_2\text{-NPs}$ Immobilized onto a Patterned Polystyrene Surface. The immobilization of $\text{NH}_2\text{-NPs}$ was finally attempted onto an insulating surface. A patterned polystyrene surface was chosen because of the numerous biological applications of polystyrene. The patterns may be obtained by local oxidation of the polystyrene surface by Ag(II) electro-generated at a SECM tip.³⁵ Such Ag(II) treatment performed on a Petri dish (not treated to favor biological cells adhesion)

generates discriminative surfaces able to promote or disfavor the adhesion of proteins and also the adhesion and growth of adherent cells.³⁵ With NPs present between the modified surface and the biological cells, hyperthermia activation of the NPs could trigger cellular death.³⁶

Here, to allow IRRAS characterization, polystyrene surfaces were polystyrene films grown from gold wafers by surface-initiated ATRP of styrene. A 250 μm diameter electrode was used to obtain a $\sim 500\text{-}\mu\text{m}$ -diameter pattern, on which any chemical change will be easily evidenced. The local polystyrene oxidation results in oxygenated functions, among which are carboxylic functions, which are expected to react with NH_2 -NPs.

The patterned polystyrene surface was submitted to the same NH_2 -NPs immobilization step as that used with gold wafers functionalized by 4-carboxyphenyl diazonium. The SEM image in Figure 4A shows that the NH_2 -NPs are preferentially

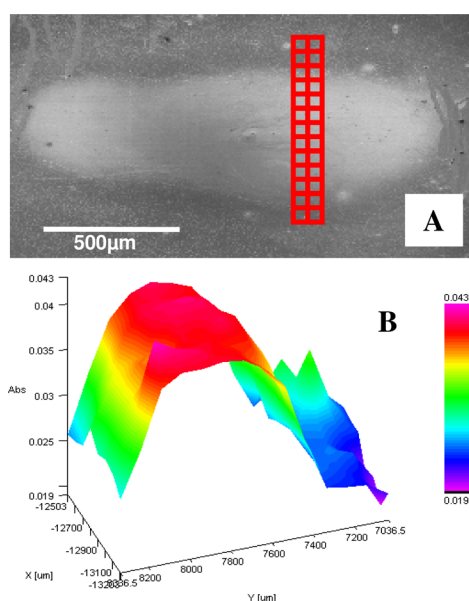


Figure 4. SEM (A) and IRRAS (B) images of $\gamma\text{-Fe}_2\text{O}_3\text{@SiO}_2$ NPs immobilized onto a patterned polystyrene surface (Pt tip biased at 2.09 V vs Pt; scan rate: 5 $\mu\text{m/s}$; tip–surface distance: 10 μm). The three-dimensional IRRAS image in (B) was obtained in the red frame in (A).

immobilized onto the electrochemically oxidized pattern. This is confirmed by the IRRAS image in Figure 4B. Such an image, that was taken in the red grid in Figure 4A, represents the intensity of the 1150 cm^{-1} band (Si–O) in a $1 \times 1\text{ mm}^2$ zone. Indeed, the absorbance is higher inside the patterned zone.

Immobilized NH_2 -NPs Functionalization. One area of interest for immobilizing NPs onto substrates is to synthesize unsymmetrical Janus NPs. Due to their unsymmetrical character, such NPs allow us to handle colloidal or biological objects in particular ways; they also allow to achieve controlled assembly and tunable optic and electronic properties.³⁷

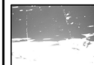
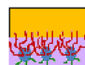
For that, after immobilization onto a surface, the NPs have to be functionalized. Then, the NP area facing the surface is unchanged, while the other face is functionalized and a Janus NP is obtained. Here, such functionalization is tested with a gold substrate modified by NH_2 -NPs, Au-NH_2 -NP. It is reacted with a fluorescent moiety substituted by a COOH group: either fluorescein or a more complex structure, such as fluorescent NPs, COOH-FNPs. Two types of combinations will be

studied: either electrostatic interactions between the NH_3^+ function from the NH_2 -NPs and the COO^- groups, or covalent bond formation via the reaction between the amino functions of the NP and the COOH functions.

At pH = 7.4 (PBS buffer), the mixing of the NH_2 -NPs with fluorescein or COOH-FNPs results in electrostatic interactions. The formation of adducts by covalent bonds was also tested. Regarding the small molecule, fluorescein isothiocyanate (FITC) was used instead of fluorescein to give a thiourea bond with the NH_2 -NPs. For the COOH-substituted fluorescent NPs, the COOH function was activated into an ester (with EDC and NHS) to give an amide function by reaction with NH_2 -NP.

Fluorescence was the most sensitive method to detect such a step. IRRAS was difficult to use to probe the coupling reaction with the fluorescein tag because of the high intensity of the Si–O band in the pertinent spectral region. The fluorescence intensities are reported in Table 2 for both modifiers and both

Table 2. Functionalization of $\gamma\text{-Fe}_2\text{O}_3\text{@SiO}_2\text{NH}_2$ -NPs Immobilized onto a Gold Surface by Fluorescein or COOH-FNPs

Immobilization of	Gray gain level (black=0 ; white= 255)	
	Fluorescein	COOH-FNP
Electrostatic interactions	40	25
	170	50
Covalent bond		

^aImage of a gold wafer covalently functionalized on half of its surface area (left: experimental, right: scheme).

types of combinations. In all cases, some fluorescence is detected, which proves that the immobilization is always effective. The fluorescence intensity is higher when a covalent bond is created instead of electrostatic interactions, as expected for a better immobilization on the NH_2 -NP composite surface. Moreover, the difference between the immobilization procedures by electrostatic interactions or by covalent bonds is lower for COOH-FNP than for fluorescein. This is related to the polyelectrolyte nature of the NPs, which then possess a large number of electrostatic anchoring sites that confer more robust electrostatic anchorage. The fluorescence response after fluorescein derivatization is higher than that with the COOH-FNP. Owing to the size difference between the molecular and NP fluorescent tags, a higher surface concentration of molecular fluorescein than of FNP is expected. However, it is difficult to go into a deeper analysis, which requires the comparison of the fluorescence efficiencies of fluorescein either in its surface confined form or when confined and encapsulated in the COOH-FNP nanoparticles.

The immobilization of COOH-FNP onto a first layer of NH_2 -NP was confirmed by different characterization methods such as the IRRAS signal at 1150 cm^{-1} for Si–O, the layer thickness measured by ellipsometry, and the surface coverage estimated by SEM (not shown). All of them increase by $\sim 20\%$ when the second layer has been immobilized via covalent interactions.

Some preliminary experiments were performed to detach the NH_2 -NPs layer from the surface by breaking the interactions between the grafted surface and the NH_2 -NPs. Classical rinsing

tests in water or solvents under stirring and/or sonication were unsuccessful. This was attested from the small decrease (<10%) of the IR absorbance signal (characteristic of the signature of the SiO₂ shell) or of fluorescence signals (characteristic of the core structure where the fluorescent tag was encapsulated for F-NH₂NPs) after these attempts. This emphasizes the strong character of the interactions between the surface and the NPs and also the good chemical and mechanical stability of the NPs layer on the substrates.

CONCLUSION

Core-shell γ -Fe₂O₃@SiO₂ NPs substituted by PEG and NH₂ groups may be immobilized onto metal surfaces via successive steps starting from the simple and efficient electrografting of a diazonium salt. The immobilization is strong enough to withstand various rinsing steps and sonication. This process has been evidenced on glassy carbon and gold. The extension to other metals, in particular, iron, should be feasible, in principle, based on previous results.⁶³

In addition to classical physical means (IRRAS, SEM, ellipsometry, or AFM), the immobilization steps are controlled by electrochemical methods (cyclic voltammetry or scanning electrochemical microscopy) that give insights into the mass transfer and charge transfer attenuation at the surface brought by each immobilization step. Electrochemical methods have generally been used to describe arrangements of conducting or catalytic nanoparticles.⁶⁴ Here, they allow us to describe, from mass-transfer perturbation, the nature of the nanoparticles layer even though they are not conducting. The method should be implemented to characterize any materials or surfaces made of assemblies of nonredox nanoparticles.

The NH₂-NPs immobilization is extended to an insulating surface such as polystyrene previously patterned by electrochemical oxidation to generate carboxylic functions. The same procedure as that carried out with glassy carbon or gold allows selectively immobilizing NH₂-NPs onto the hydrophilic patterns. These preliminary results should be confirmed directly in a Petri dish (not treated for cell adhesion) with smaller patterns whose size compares to that of biological cells. Based on the good mechanical and chemical stability of the NPs layer which strongly adheres to the substrates, such systems may find applications for hyperthermia activation of the NPs to trigger cellular death.³⁶

Finally, the chemical reactivity of the immobilized NPs is tested through coupling with fluorescent moieties (fluorescein) or nanoparticles (COOH-FNPs). This strategy leads to the formation of Janus NPs once the NPs are detached from the surface, for applications in colloids, biology, optics, electronics, and so forth. Future work will be dedicated to the recovery of the Janus NPs from the substrate surface. This step is difficult to achieve because of the strong interaction between the grafted surface and the first NPs layer. Attempts are presently in progress, for example, by performing all reactions in a microfluidic channel and also by using pH changes to favor immobilization or separation.

ASSOCIATED CONTENT

Supporting Information

Additional figures. This material is available free of charge via the Internet at <http://pubs.acs.org>.

AUTHOR INFORMATION

Corresponding Author

*E-mail: catherine.combellas@espci.fr.

Notes

The authors declare no competing financial interest.

ACKNOWLEDGMENTS

The "Agence Nationale de la Recherche" is gratefully acknowledged for its financial support via the ANR-06-BLAN-0368 project.

REFERENCES

- (1) Whitesides, G. M. The 'right' size in nanobiotechnology. *Nat. Biotechnol.* **2003**, *21*, 1161–1165.
- (2) Shipway, A. N.; Katz, E.; Willner, I. Nanoparticle arrays on surfaces for electronic, optical, and sensor applications. *ChemPhysChem* **2000**, *1*, 18–52.
- (3) Michalet, X.; Pinaud, F. F.; Bentolila, L. A.; Tsay, J. M.; Doose, S.; Li, J. J.; Sundaresan, G.; Wu, A. M.; Gambhir, S. S.; Weiss, S. Quantum dots for live cells, in vivo imaging, and diagnostics. *Science* **2005**, *307*, 538–544.
- (4) Biju, V.; Itoh, T.; Ishikawa, M. Delivering quantum dots to cells: bioconjugated quantum dots for targeted and nonspecific extracellular and intracellular imaging. *Chem. Soc. Rev.* **2010**, *39*, 3031–3056.
- (5) Wang, F.; Banerjee, D.; Liu, Y. S.; Chen, X. Y.; Liu, X. G. Upconversion nanoparticles in biological labeling, imaging, and therapy. *Analyst* **2010**, *135*, 1839–1854.
- (6) Agrawal, M.; Pich, A.; Zafeiropoulos, N. E.; Gupta, S.; Pionteck, J.; Simon, F.; Stamm, M. Polystyrene-ZnO composite particles with controlled morphology. *Chem. Mater.* **2007**, *19*, 1845–1852.
- (7) Klein, D. L.; Roth, R.; Lim, A. K. L.; Alivisatos, A. P.; McEuen, P. L. A single-electron transistor made from a cadmium selenide nanocrystal. *Nature* **1997**, *389*, 699–701.
- (8) Kiely, C. J.; Fink, J.; Brust, M.; Bethell, D.; Schiffrin, D. J. Spontaneous ordering of bimodal ensembles of nanoscopic gold clusters. *Nature* **1998**, *396*, 444–446.
- (9) Taton, T. A.; Mucic, R. C.; Mirkin, C. A.; Letsinger, R. L. The DNA-mediated formation of supramolecular mono- and multilayered nanoparticle structures. *J. Am. Chem. Soc.* **2000**, *122*, 6305–6306.
- (10) Teste, B.; Descroix, S. Colloidal nanomaterial-based immunoassay. *Nanomedicine* **2012**, *7*, 917–929.
- (11) Goss, C. A.; Charych, D. H.; Majda, M. Application of (3-mercaptopropyl)trimethoxysilane as a molecular adhesive in the fabrication of vapor-deposited gold electrodes on glass substrates. *Anal. Chem.* **1991**, *63*, 85–88.
- (12) Chumanov, G.; Sokolov, K.; Gregory, B. W. Colloidal metal-films as a substrate for surface enhanced spectroscopy. *J. Phys. Chem.* **1995**, *99*, 9466–9471.
- (13) Freeman, R. G.; Grabar, K. C.; Allison, K. J.; Bright, R. M.; Davis, J. A.; Guthrie, A. P.; Hommer, M. B.; Jackson, M. A.; Smith, P. C.; Walter, D. G.; Natan, M. J. Self-assembled metal colloid monolayers-An approach to SERS substrates. *Science* **1995**, *267*, 1629–1632.
- (14) Grabar, K. C.; Freeman, R. G.; Hommer, M. B.; Natan, M. J. Preparation and characterization of Au colloid monolayers. *Anal. Chem.* **1995**, *67*, 735–743.
- (15) Shavel, A.; Gaponik, N.; Eychemuller, A. Covalent linking of CdTe nanocrystals to amino-functionalized surfaces. *ChemPhysChem* **2005**, *6*, 449–451.
- (16) Brust, M.; Walker, M.; Bethell, D.; Schiffrin, D. J.; Whyman, R. Synthesis of thiol-derivatized gold nanoparticles in a 2-phase liquid-liquid system. *J. Chem. Soc.: Chem. Commun.* **1994**, *7*, 801–802.
- (17) Levy, R.; Thanh, N. T. K.; Doty, R. C.; Hussain, I.; Nichols, R. J.; Schiffrin, D. J.; Brust, M.; Fernig, D. G. Rational and combinatorial design of peptide capping ligands for gold nanoparticles. *J. Am. Chem. Soc.* **2004**, *126*, 10076–10084.

- (18) Brust, M.; Bethell, D.; Kiely, C. J.; Schiffrin, D. J. Self-assembled gold nanoparticle thin films with nonmetallic optical and electronic properties. *Langmuir* **1998**, *14*, 5425–5429.
- (19) Yamanoi, Y.; Yonezawa, T.; Shirahata, N.; Nishihara, H. Immobilization of gold nanoparticles onto silicon surfaces by Si-C covalent bonds. *Langmuir* **2004**, *20*, 1054–1056.
- (20) Decher, G. Fuzzy nanoassemblies: Toward layered polymeric multicomposites. *Science* **1997**, *277*, 1232–1237.
- (21) Kotov, N. A.; Dekany, I.; Fendler, J. H. Layer-by-layer self assembly of polyelectrolyte-semiconductor nanoparticle composite films. *J. Phys. Chem.* **1995**, *99*, 13065–13069.
- (22) Lvov, Y.; Ariga, K.; Onda, M.; Ichinose, I.; Kunitake, T. Alternate assembly of ordered multilayers of SiO₂ and other nanoparticles and polyions. *Langmuir* **1997**, *13*, 6195–6203.
- (23) Lvov, Y.; Ariga, K.; Onda, M.; Ichinose, I.; Kunitake, T. A careful examination of the adsorption step in the alternate layer-by-layer assembly of linear polyanion and polycation. *Colloids Surf., A: Physicochem. Eng. Aspects* **1999**, *146*, 337–346.
- (24) Ostrander, J. W.; Mamedov, A. A.; Kotov, N. A. Two modes of linear layer-by-layer growth of nanoparticle-polyelectrolyte multilayers and different interactions in the layer-by-layer deposition. *J. Am. Chem. Soc.* **2001**, *123*, 1101–1110.
- (25) Delamar, M.; Hitmi, R.; Pinson, J.; Savéant, J.-M. Covalent modification of carbon surfaces by grafting of functionalized aryl radicals produced from electrochemical reduction of diazonium salts. *J. Am. Chem. Soc.* **1992**, *114*, 5883–5884.
- (26) Adenier, A.; Bernard, M. C.; Chehimi, M. M.; Cabet-Deliry, E.; Desbat, B.; Fagebaume, O.; Pinson, J.; Podvorica, F. Covalent modification of iron surfaces by electrochemical reduction of aryldiazonium salts. *J. Am. Chem. Soc.* **2001**, *123*, 4541–4549.
- (27) deVilleneuve, C. H.; Pinson, J.; Bernard, M. C.; Allongue, P. Electrochemical formation of close-packed phenyl layers on Si(111). *J. Phys. Chem. B* **1997**, *101*, 2415–2420.
- (28) Dyke, C. A.; Tour, J. M. Solvent-free functionalization of carbon nanotubes. *J. Am. Chem. Soc.* **2003**, *125*, 1156–1157.
- (29) Jian, W.; Firestone, M. A.; Auciello, O.; Carlisle, J. A. Surface functionalization of ultrananocrystalline diamond films by electrochemical reduction of aryldiazonium salts. *Langmuir* **2004**, *20*, 11450–11456.
- (30) Combellas, C.; Kanoufi, F.; Mazouzi, D.; Thiebault, A.; Bertrand, P.; Medard, N. Surface modification of halogenated polymers. 4. Functionalisation of poly(tetrafluoroethylene) surfaces by diazonium salts. *Polymer* **2003**, *44*, 19–24.
- (31) Harnisch, J. A.; Pris, A. D.; Porter, M. D. *J. Am. Chem. Soc.* **2001**, *123*, 5829–5830.
- (32) Noel, J.-M.; Zigah, D.; Simonet, J.; Hapiot, P. Attachment of gold nanoparticles to glassy carbon electrodes via a mercaptobenzene film. Synthesis and Immobilization of Ag-0 Nanoparticles on Diazonium Modified Electrodes: SECM and Cyclic Voltammetry Studies of the Modified Interfaces. *Langmuir* **2010**, *26*, 7638–7643.
- (33) Gehan, H.; Fillaud, L.; Felidj, N.; Aubard, J.; Lang, P.; Chehimi, M. M.; Mangeney, C. A General Approach Combining Diazonium Salts and Click Chemistries for Gold Surface Functionalization by Nanoparticle Assemblies. *Langmuir* **2010**, *26*, 3975–3980.
- (34) Joyeux, X.; Ammar, S.; Dijon, J.; Pinson, J. Growth of carbon nanotubes through selective deposition of nanoparticles. *J. Mater. Chem.* **2010**, *20*, 7197–7200.
- (35) Ktari, N.; Poncet, P.; Sénéchal, H.; Malaquin, L.; Kanoufi, F.; Combellas, C. Patterning of polystyrene by Scanning Electrochemical Microscopy. Biological applications to cell adhesion. *Langmuir* **2010**, *26*, 17348–17356.
- (36) Lee, J. H.; Jang, J. T.; Choi, J. S.; Moon, S. H.; Noh, S. H.; Kim, J. W.; Kim, J.-G.; Kim, I. S.; Park, K. I.; Cheon, J. Exchange-coupled magnetic nanoparticles for efficient heat induction. *Nat. Nanotechnol.* **2011**, *6*, 418–422.
- (37) Wang, B.; Li, B.; Zhao, B.; Li, C. Y. Amphiphilic Janus gold nanoparticles via combining "Solid-State Grafting-to" and "Grafting-from" methods. *J. Am. Chem. Soc.* **2008**, *130*, 11594–11595.
- (38) Georgelin, T.; Bombard, S.; Siaugue, J. M.; Cabuil, V. Nanoparticle-Mediated Delivery of Bleomycin. *Angew. Chem., Int. Ed.* **2010**, *49*, 8897–8901.
- (39) Bacri, J. C.; Perzynski, R.; Salin, D.; Cabuil, V.; Massart, R. Magnetic colloidal properties of ionic ferrofluids. *J. Magn. Magn. Mater.* **1986**, *62*, 36–46.
- (40) Laurencin, M.; Georgelin, T.; Malezieux, B.; Siaugue, J. M.; Menager, C. Interactions Between Giant Unilamellar Vesicles and Charged Core-Shell Magnetic Nanoparticles. *Langmuir* **2010**, *26*, 16025–16030.
- (41) d'Orlye, F.; Varenne, A.; Georgelin, T.; Siaugue, J.-M.; Teste, B.; Descroix, S.; Gareil, P. Charge-based characterization of nanometric cationic bifunctional maghemite/silica core/shell particles by capillary zone electrophoresis. *Electrophoresis* **2009**, *30*, 2572–2582.
- (42) Matrab, T.; Hauquier, F.; Combellas, C.; Kanoufi, F. Cyclic voltammetry and scanning electrochemical microscopy investigation of molecular transport and reactivity within polymer brushes. Consequences for the patterning of polymer brushes surfaces. *ChemPhysChem* **2010**, *11*, 670–682.
- (43) Matrab, T.; Chehimi, M. M.; Perruchot, C.; Adenier, A.; Guillez, V.; Save, M.; Charleux, B.; Cabet-Deliry, E.; Pinson, J. Novel approach for metallic surface-initiated atom transfer radical polymerization using electrografted initiators based on aryl diazonium salts. *Langmuir* **2005**, *21*, 4686–4694.
- (44) Combellas, C.; Ghilane, J.; Kanoufi, F.; Mazouzi, D. Surface modification of halogenated polymers. 7. Local reduction of poly(tetrafluoroethylene) and poly(chlorotrifluoroethylene) by a scanning electrochemical microscope in the feedback mode. *J. Phys. Chem. B* **2004**, *108*, 6391–6397.
- (45) Combellas, C.; Kanoufi, F.; Mazouzi, D. Surface modification of halogenated polymers. 8. Local reduction of poly(tetrafluoroethylene) by the scanning electrochemical microscope - Transient investigation. *J. Phys. Chem.* **2004**, *108*, 19260–19268.
- (46) Combellas, C.; Kanoufi, F.; Mazouzi, D. Surface modification of halogenated polymers. 9. Etching of polytetrafluoroethylene with the scanning electrochemical microscope. *J. Electroanal. Chem.* **2006**, *589*, 243–248.
- (47) Lefrou, C.; Cornut, R. New analytical approximation of feedback approach curves with a microdisk SECM tip and irreversible kinetic reaction at the substrate. *J. Electroanal. Chem.* **2008**, *621*, 178–184.
- (48) Ktari, N.; Combellas, C.; Kanoufi, F. Local Oxidation of Polystyrene by Scanning Electrochemical Microscopy. *J. Phys. Chem. C* **2011**, *115*, 17891–17897.
- (49) Hauquier, F.; Matrab, T.; Kanoufi, F.; Combellas, C. Local direct and indirect reduction of electrografted aryldiazonium/gold surfaces for polymer brushes patterning. *Electrochim. Acta* **2009**, *54*, 5127–5136.
- (50) Gueshi, T.; Tokuda, K.; Matsuda, H. Voltammetry at partially covered electrodes. 2. Linear potential sweep and cyclic voltammetry. *J. Electroanal. Chem.* **1979**, *101*, 29–38.
- (51) Amatore, C.; Saveant, J. M.; Tessier, D. Charge transfer at partially blocked surfaces- A model for the case of microscopic active and inactive sites. *J. Electroanal. Chem.* **1983**, *147*, 39–51.
- (52) Davies, T. J.; Compton, R. G. The cyclic and linear sweep voltammetry of regular and random arrays of microdisc electrodes: Theory. *J. Electroanal. Chem.* **2005**, *585*, 63–82.
- (53) Davies, T. J.; Moore, R. R.; Banks, C. E.; Compton, R. G. The cyclic voltammetric response of electrochemically heterogeneous surfaces. *J. Electroanal. Chem.* **2004**, *574*, 123–152.
- (54) Davies, T. J.; Lowe, E. R.; Wilkins, S. J.; Compton, R. G. Voltammetric sizing of inert particles. *ChemPhysChem* **2005**, *6*, 1340–1347.
- (55) Nicholson, R. S. Theory and application of cyclic voltammetry for measurement of electrode reaction kinetics. *Anal. Chem.* **1965**, *37*, 1351–1355.
- (56) Baranton, S.; Belanger, D. Electrochemical derivatization of carbon surface by reduction of in situ generated diazonium cations. *J. Phys. Chem. B* **2005**, *109*, 24401–24410.

(57) (a) The dimensionless peak current for a 1-electron reversible ET is $\psi_p = i_p / (FAC^0(DFv/RT)^{1/2})$ 0.446 and tends toward $\psi_p = 0.496 \alpha^{1/2}$ for an irreversible ET with charge transfer coefficient α (for $\text{Fe}(\text{CN})_6^{4/3-}$ $\alpha = 0.5$); F is the Faraday, A the electrode area, C^0 the redox probe bulk concentration, D the diffusivity, v the scan rate, R the gas constant, and T the temperature. (b) Bard, A. J., and Faulkner, L. R. *Electrochemical methods: Fundamentals and Applications*, 2nd ed.; Wiley: New York, 2001.

(58) Newton, M. R.; Morey, K. A.; Zhang, Y.; Snow, R. J.; Diwekar, M.; Shi, J.; White, H. S. Anisotropic diffusion in face-centered cubic opals. *Nano Lett.* **2004**, *4*, 875–880.

(59) Paulik, M. G.; Brooksby, P. A.; Abell, A. D.; Downard, A. J. Grafting aryl diazonium cations to polycrystalline gold: Insights into film structure using gold oxide reduction, redox probe electrochemistry, and contact angle behavior. *J. Phys. Chem. C* **2007**, *111*, 7808–7815.

(60) Forouzan, F.; Bard, A. J.; Mirkin, M. V. Voltammetric and scanning electrochemical microscopic studies of the adsorption kinetics and self-assembly of n-alkanethiol monolayers on gold. *Isr. J. Chem.* **1997**, *37*, 155–163.

(61) Kim, E.; Xiong, H.; Striemer, C. C.; Fang, D. Z.; Fauchet, P. M.; McGrath, J. L.; Amemiya, S. A structure-permeability relationship of ultrathin nanoporous silicon membrane: a comparison with the nuclear envelope. *J. Am. Chem. Soc.* **2008**, *130*, 4230–4231.

(62) Maurice, V.; Georgelin, T.; Siaugue, J.-M.; Cabuil, V. Synthesis and characterization of functionalized core-shell gamma Fe_2O_3 - SiO_2 nanoparticles. *J. Magn. Magn. Mater.* **2009**, *321*, 1408–1413.

(63) Combellas, C.; Delamar, M.; Kanoufi, F.; Pinson, J.; Podvorica, F. I. Spontaneous grafting of iron surfaces by reduction of aryldiazonium salts in acidic or neutral aqueous solution. Application to the protection of iron against corrosion. *Chem. Mater.* **2005**, *17*, 3968–3975.

(64) Murray, R. W. Nanoelectrochemistry: metal nanoparticles, nanoelectrodes, and nanopores. *Chem. Rev.* **2008**, *108*, 2688–2720.